Measurements of nitrogen dioxide total column amounts using a Brewer double spectrophotometer in direct Sun mode

Alexander Cede,[1,2] Jay Herman,[2] Andreas Richter,[3] Nickolay Krotkov,[2,4] and John Burrows[3]

Received 12 August 2005; revised 1 November 2005; accepted 23 November 2005; published 2 March 2006.

[1] NO_2 column amounts were measured for the past 2 years at Goddard Space Flight Center, Greenbelt, Maryland, using a Brewer spectrometer in direct Sun mode. A new "bootstrap" method to calibrate the instrument is introduced and described. This technique selects the cleanest days from the database to obtain the solar reference spectrum. The main advantage for direct Sun measurements is that the conversion uncertainty from slant column to vertical column is negligible compared to the standard scattered light observations where it is typically on the order of 100% (2σ) at polluted sites. The total 2σ errors of the direct Sun retrieved column amounts decrease with solar zenith angle and are estimated at 0.2 to 0.6 Dobson units (DU, 1 DU $\approx 2.7 \times 10^{16}$ molecules cm^{-2}), which is more accurate than scattered light measurements for high NO_2 amounts. Measured NO_2 column amounts, ranging from 0 to 3 DU with a mean of 0.7 DU, show a pronounced daily course and a strong variability from day to day. The NO_2 concentration typically increases from sunrise to noon. In the afternoon it decreases in summer and stays constant in winter. As expected from the anthropogenic nature of its source, NO_2 amounts on weekends are significantly reduced. The measurements were compared to satellite retrievals from Scanning Image Absorption Spectrometer for Atmospheric Chartography (SCIAMACHY). Satellite data give the same average NO_2 column and show a seasonal cycle that is similar to the ground data in the afternoon. We show that NO_2 must be considered when retrieving aerosol absorption properties, especially for situations with low aerosol optical depth.

Citation: Cede, A., J. Herman, A. Richter, N. Krotkov, and J. Burrows (2006), Measurements of nitrogen dioxide total column amounts using a Brewer double spectrophotometer in direct Sun mode, *J. Geophys. Res.*, *111*, D05304, doi:10.1029/2005JD006585.

1. Introduction

[2] Nitrogen dioxide (NO_2) is a key species in the chemistry of both the stratosphere and troposphere. It is one of the most important ozone precursors in the troposphere and locally also contributes to radiative forcing [*Solomon et al.*, 1999]. In addition, it is known to cause human respiratory problems [e.g., *Environmental Protection Agency*, 1998]. The majority of atmospheric NO_2 is produced by anthropogenic sources. Industry and traffic produce about 50%, and biomass burning is estimated to contribute about 20%. Other important sources are lightning ($\sim$10%) and emissions from soil ($\sim$15%) [*Lee et al.*, 1997]. Stratospheric NO_2 shows a diurnal cycle with maximum concentrations around sunset and a seasonal cycle with maxima in summer and larger abundance at midlatitudes and high latitudes than in the tropics [*Noxon*, 1979; *Van Roozendael et al.*, 1997; *Liley et al.*, 2000]. In midlatitudes the stratospheric column of NO_2 varies roughly between 0.05 and 0.25 Dobson units (DU); 1 DU corresponds to a column density of $\sim 2.7 \times 10^{16}$ cm^{-2}. Quantity and temporal behavior of tropospheric NO_2 are less known. Column amounts of tropospheric NO_2 between 0 and more than 2 DU have been estimated from ground-based column measurements [*Brewer et al.*, 1973], from satellite retrievals [*Richter and Burrows*, 2002], and from in situ measurements converted into column amounts by means of chemical transport models [*Petritoli et al.*, 2004; *Ordóñez et al.*, 2006]. Satellite data, in situ measurements, and calculations with chemical transport models show seasonal cycles of tropospheric NO_2 with maximum amounts in winter [*Velders et al.*, 2001; *Petritoli et al.*, 2004; *Ordóñez et al.*, 2006].

[3] Remote sensing measurements of atmospheric NO_2 from the ground are usually performed using differential optical absorption spectroscopy (DOAS) [*Platt*, 1994] of scattered sunlight. In this technique the spectral sky radiance is measured, and the slant column density of the

[1] Science Systems and Applications Incorporated, Lanham, Maryland, USA.
[2] NASA Goddard Space Flight Center, Greenbelt, Maryland, USA.
[3] Institute of Environmental Physics, University of Bremen, Bremen, Germany.
[4] Goddard Earth Science and Technology Center, University of Maryland Baltimore County, Catonsville, Maryland, USA.

0148-0227/06/2005JD006585$09.00

atmospheric species is derived from differential absorption structures using Lambert-Beer's law. The slant column is then divided by the estimated air mass factor (AMF) to obtain the vertical column. The sky radiance is measured either in zenith direction (zenith sky DOAS) [e.g., *Van Roozendael et al.*, 1997; *Liley et al.*, 2000] or in multiple directions (multiaxis DOAS, MAXDOAS) [e.g., *Leser et al.*, 2003]. Zenith sky DOAS is usually performed for large solar zenith angles (SZA) during sunrise and sunset and is mainly sensitive to stratospheric NO_2. The reference spectrum, used to remove the solar Fraunhofer structure, is normally obtained from measurements at low SZA during the same day. In contrast, MAXDOAS is mainly sensitive to tropospheric NO_2 with the reference spectrum taken from the zenith direction. DOAS techniques are also used for aircraft measurements [e.g., *Heue et al.*, 2005] and for satellite measurements [e.g., *Leue et al.*, 2001; *Richter et al.*, 2004]. Satellite measurements usually obtain their reference spectrum directly from the Sun.

[4] All scattered light DOAS methods require sophisticated radiative transfer calculations within a model atmosphere to estimate the AMF and have to include the Ring effect in the analysis [*Solomon et al.*, 1987]. The large AMF in scattered light measurements decreases the influence of the reference spectrum and gives a strong NO_2 signal, which increases sensitivity for small amounts of NO_2. Intercomparisons of slant column densities of NO_2 derived from zenith sky DOAS measurements normally show less than 10% differences from instrument to instrument with clear-sky conditions [*Roscoe et al.*, 1999; *Vandaele et al.*, 2005]. However, in particular for satellite observations the theoretical determination of the AMF depends on several atmospheric parameters such as the vertical NO_2 profile, aerosols, clouds, and surface albedo. Therefore, even for clear-sky conditions, the uncertainty in the satellite AMF for polluted regions is very high, typically around 100%, which is the largest uncertainty source for scattered light DOAS [*Heland et al.*, 2002; *Boersma et al.*, 2004]. This is a two standard deviation uncertainty (2σ) level, which will be used for all uncertainties given in this paper.

[5] The direct Sun technique for deriving vertical column NO_2 is equally sensitive to stratospheric and tropospheric NO_2, does not require sophisticated radiative transfer calculations, and is not affected by the Ring effect. More importantly, the influence of atmospheric parameters on the AMF for direct Sun measurements is very small (less than 1% for SZA $< 80°$). However, the comparatively small AMF causes rather small NO_2 signals. Unlike zenith sky DOAS or MAXDOAS, a major problem for direct Sun observations is calibration of the instrument and determination of the reference spectrum. Previously, *Brewer et al.* [1973] measured NO_2 with a variety of techniques, including direct Sun, from ground and aircraft in Toronto, Canada, and reported variations of the total (equal to tropospheric plus stratospheric) vertical column from 0.3 to 3 DU. The Brewer MK4 single-monochromator type [*Kerr et al.*, 1985] includes the possibility of measuring NO_2 using the grating's second order of scattering between 428 and 453 nm [e.g., *Francesconi et al.*, 2004]. There is still debate in the literature regarding the possibility of deriving NO_2 from filter Sun photometer measurements [*Rublev et al.*, 2003].

[6] In this paper we present 2 years of measurements of total column NO_2 near Washington, D. C., obtained using a Brewer MK3 double monochromator in direct Sun mode. We give details for the algorithm and calibration technique that were used. We show selected results and a comparison with satellite data from Scanning Imaging Absorption Spectrometer for Atmospheric Chartography (SCIAMACHY) [*Burrows et al.*, 1995], and we analyze the temporal and spatial behavior of NO_2. We also show the influence of high NO_2 levels on the determination of aerosol absorption properties.

2. Materials and Methods

2.1. Instrument

[7] The measurements were performed at Goddard Space Flight Center (GSFC), Greenbelt, Maryland (38.98°N, 76.83°W, 90 m above sea level), using a Brewer MK3 spectrometer [*Kerr et al.*, 1985]. Our instrument, Brewer 171, has a wavelength range from 282.6 to 363.6 nm and a triangular slit function with full width at half maximum from 0.47 to 0.67 nm that decreases with wavelength. Brewer 171 is a double monochromator with very low internal stray light ($<10^{-8}$) and therefore ideal for measurements in the ultraviolet (UV), especially for wavelengths less than 320 nm, which we are using for ozone (O_3) and sulfur dioxide (SO_2) retrievals. Brewer spectrometers are widely used all over the world, mostly to derive total ozone column from a narrow field of view port and global UV irradiance from a separate entrance port using a Teflon diffuser. In the data reduction the raw counts of the Brewer are converted to "effective count rates," which include corrections for the dark count, the internal attenuation filters used to adjust the intensity, the dead time of the photomultiplier tube, and the instrument's temperature dependence. The narrow field of view port of Brewer 171 was absolutely calibrated in our laboratory in the same way as described by *Kazadzis et al.* [2005].

[8] The Brewer can operate either in a "scanning mode," where the gratings are moved and any wavelength can be selected, or in a "slit mask mode," which allows nearly simultaneous measurements of six wavelengths, which are about 3 nm apart, at fixed grating position. In the slit mask mode the measured signals are obtained from multiple runs over all six wavelengths with 0.1147 s integration time for each wavelength. For our NO_2 retrievals we used a "short" and a "long" measurement routine. The short routine consists of five sets of 4 repetitions at each wavelength, giving a total of about 2.3 s integration time per wavelength. In the long routine the repetitions are increased to 16, which results in 4 times more integration time ($\sim$9.2 s).

2.2. Algorithm

[9] Figure 1 (top) shows typical optical depths of the main atmospheric trace gases that absorb in the Brewer's wavelength range. O_3 and SO_2 column amounts can be retrieved from our Brewer spectrometer measurements in the wavelength range between 303 and 320 nm. The averages of the measured column amounts at our location are 315 and 1.2 DU for O_3 and SO_2, respectively. At our site we estimate a maximum amount of total formaldehyde (HCHO) of 2 DU [*Heckel et al.*, 2005], and we estimate

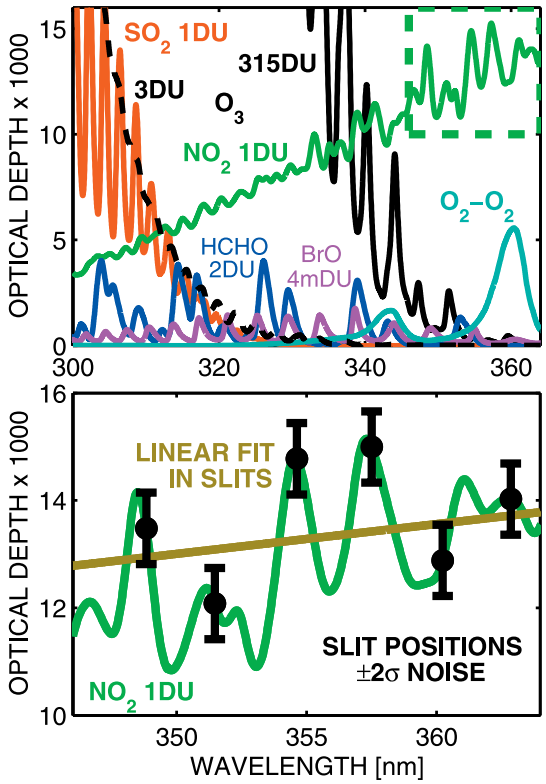

Figure 1. (top) Typical optical depths of the main trace gases in the instrument's wavelength range (solid lines). The dashed black line is for 3 DU of ozone to illustrate the influence of a 1% total ozone retrieval error. (bottom) NO_2 optical depth for 1 DU, six slit positions (black dots) with noise estimations, and linear fit in slits.

the bromine oxide (BrO) amount not to exceed 0.004 DU [*Leser et al.*, 2003]. The oxygen dimer (O_2-O_2) optical depth in Figure 1 is for 1 atm pressure.

[10] All optical depths given in Figure 1 are calculated from an altitude integral using temperature-dependent cross sections with a yearly average temperature profile corresponding to the location's latitude, and the depths are convoluted with the instrument's slit function. The absorption cross sections for NO_2, O_3, SO_2, HCHO, BrO, and O_2-O_2 are taken from *Vandaele et al.* [1998], *Burrows et al.* [1999], *Vandaele et al.* [1994], *Meller and Moortgat* [2000], *Wilmouth et al.* [1999], and *Greenblatt et al.* [1990], respectively.

[11] The wavelength range used for the NO_2 retrieval is marked in Figure 1 (top, dashed green box) and magnified in Figure 1 (bottom). In this wavelength region the highest (gaseous) absorption optical depths, aside from NO_2, are from O_2-O_2 and ozone. HCHO and BrO show some minor influence, and SO_2 does not absorb at all. The six black dots in Figure 1 (bottom) show the six wavelengths used for the NO_2 retrieval in the slit mask mode (air wavelengths 348.83, 351.47, 354.62, 357.51, 360.24, and 362.86 nm). The brown line represents a linear least squares fit to the black dots. Slits 1 and 6 are approximately on this linear fit, slits 2 and 5 are below the fit, and slits 3 and 4 are above it. The differences of the NO_2 optical depths for 1 DU relative to the linear fit are $+0.1 \times 10^{-3}$, -1.4×10^{-3}, $+1.2 \times 10^{-3}$, $+1.2 \times 10^{-3}$, -1.1×10^{-3}, and -0.1×10^{-3} for slits 1 to 6, respectively. This means that for 1 DU of total column NO_2 and AMF = 1 (SZA = 0°) the differential signal in the slits is about +0.1% at slits 3 and 4 and about −0.1% at slits 2 and 5. The instrumental noise estimates for the long measurement routine and typical count rates of about 10^6 s^{-1} are shown as vertical lines (converted to optical depth for AMF = 1).

[12] The algorithm to derive NO_2 is based on the following equation. For each wavelength we can write

$$F = F_0 e^{-m\tau} + \Delta F_{SCATT}, \tag{1}$$

where F is the measured irradiance, F_0 is the irradiance at the top of the atmosphere, m is the AMF, τ is the total vertical optical depth (see Figure 1), and ΔF_{SCATT} is the small amount of the diffuse irradiance entering the field of view. The product of AMF and optical depth in (1) is a sum of different terms, each standing for extinction by different species. Forming the natural logarithm and rearranging (1) yields

$$\ln F_0 = \ln F + \ln(1 - r_{SCATT}) + m_{DIV}\tau_{DIV} + m_{AER}\tau_{AER} + m_{NO2}\tau_{NO2}\Omega_{NO2}, \tag{2}$$

where r_{SCATT} is the ratio $\Delta F_{SCATT}/F$. In the subscripts, AER stands for aerosols, and DIV stands for "diverse" optical depths (in our case, molecular scattering and gaseous absorption by O_3, O_2-O_2, HCHO, and BrO). The parameter τ_{NO2} is the NO_2 optical depth for 1 DU (see Figure 1), and Ω_{NO2} is the total vertical column amount of NO_2 in DU. The AMF m is calculated using

$$m = \sec\{\arcsin[k \sin(SZA)]\}, \tag{3}$$

where k is given by

$$k = R/(R + z), \tag{4}$$

where R is the Earth's radius and z is the effective layer height of the species. We used z = 8 km for molecular scattering, z = 5 km for O_2-O_2 absorption, z = 23 km for O_3 and BrO, and z = 2 km for aerosols, NO_2, and HCHO (i.e., we assume aerosols, NO_2, and HCHO to accumulate in the lower troposphere).

[13] We can estimate all variables on the right side of (2) except for r_{SCATT}, τ_{AER}, and Ω_{NO2}. For molecular scattering, we use the formula from *Bodhaine et al.* [1999] for dry air with a CO_2 content of 370 ppm and the mean surface pressure at the station. The total ozone amount is obtained from our Brewer spectrometer measurements. As mentioned at the beginning of this section, the HCHO and BrO amounts are less important at our site. However, on the basis of the maximum estimations of 2 and 0.004 DU for HCHO and BrO, respectively, we include constant estimated "mean" optical depths of 1 DU for HCHO and 0.002 DU for BrO in the algorithm for NO_2 retrieval. For both τ_{AER} and r_{SCATT} we assume a linear behavior with wavelength over this small range of 14 nm. If we knew the irradiance at the top of the atmosphere F_0, we could simultaneously fit a constant and linear aerosol term and Ω_{NO2} using

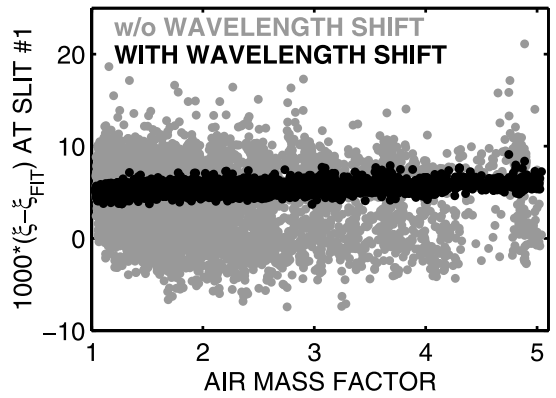

Figure 2. Residuals from 5310 cloud-screened measurements at slit 1, 349 nm, with (black dots) and without (gray dots) including a wavelength shift.

equation (2). Section 2.3 describes the calibration method we used to determine F_0.

2.3. Calibration

2.3.1. Step 1

[14] We calculated the parameter ξ at each wavelength:

$$\xi = \ln F_0' - \ln F - m_{\mathrm{DIV}}\tau_{\mathrm{DIV}} = m_{\mathrm{AER}}\tau_{\mathrm{AER}} + \ln(1 - r_{\mathrm{SCATT}}) + m_{\mathrm{NO2}}\tau_{\mathrm{NO2}}\Omega_{\mathrm{NO2}} + \Delta \ln F_0. \quad (5)$$

F_0' is a first guess for F_0, where we used the Solar Ultraviolet Spectral Irradiance Monitor (SUSIM)/Atlas 3 spectrum [*Floyd et al.*, 2003], convoluted with the Brewer slit functions and corrected for the Sun-Earth distance. The parameters m_{DIV} and τ_{DIV} are calculated as described in section 2.2. $\Delta \ln F_0$ stands for a possible systematic error in our estimation of F_0. The parameters ξ are built for the whole "calibration database," that is, 18,883 measurements from August 2003 to February 2005 (about every 20 min for SZA < 80 °).

2.3.2. Step 2

[15] Each measurement consists of five repetitions (sets) obtained for all sky conditions. To apply a cloud filter, we only kept those measurements where the value of ξ/m_{AER} (approximately aerosol optical depth) at the longest wavelength (363 nm) is less than 1 and the standard deviation over the sets is less than 0.02. This reduced the database to 5310 cloud-screened measurements.

2.3.3. Step 3

[16] We fitted a constant and linear term as a function of wavelength to ξ and subtracted the linear fit ξ_{FIT} obtaining the "residuals" $\xi - \xi_{\mathrm{FIT}}$. This procedure should eliminate effects of aerosol extinction (τ_{AER}), the fraction of diffuse irradiance entering the field of view (r_{SCATT}), and linear instrumental drifts, so that the residuals should depend, to first order, on the total NO_2 column Ω_{NO2} and $\Delta \ln F_0$.

$$\xi - \xi_{\mathrm{FIT}} = m_{\mathrm{NO2}}\tau'_{\mathrm{NO2}}\Omega_{\mathrm{NO2}} + \Delta \ln F_0', \quad (6)$$

where τ'_{NO2} is the differential optical depth of NO_2 (i.e., the difference between the green line and the brown line in Figure 1) and $\Delta \ln F_0'$ is the "differential systematic error" of F_0.

[17] The gray dots in Figure 2 show the residuals $\xi - \xi_{\mathrm{FIT}}$ at slit 1 (349 nm) as a function of the AMF m_{NO2}. The spread of the residuals is ±0.01, which is about 10 times higher than expected from noise estimations (see vertical bars in Figure 1, bottom). Furthermore, when making a singular-value decomposition of the residuals, the principal vector does not at all look like τ'_{NO2} (black solid line compared to gray line, Figure 3).

[18] Nevertheless, it turns out that the residuals at different slits are highly correlated with each other, and the correlation pattern clearly indicates that a small wavelength shift caused the high correlation and large scatter of the residuals. The wavelength calibration of the spectrometer was done as described by *Gröbner et al.* [1998], and the wavelength uncertainty for field conditions was determined to 0.015 nm, which is pretty good overall but still too large for the purpose of deriving NO_2. Using the SUSIM spectrum, we can expect variations of F_0 of up to ±1% due to wavelength shifts (gray line in Figure 4).

[19] The Brewer instrument performs wavelength checks using an internal mercury lamp several times a day and records the results of these tests. Interpolating in time, we

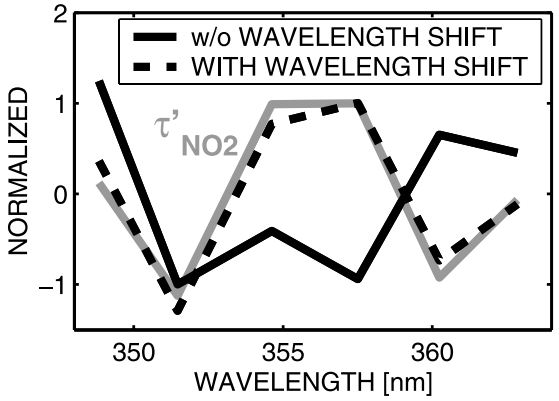

Figure 3. Differential optical depth of NO_2 (gray line) and principal vectors of singular value decomposition of the residuals with (dashed black line) and without (solid black line) including a wavelength shift.

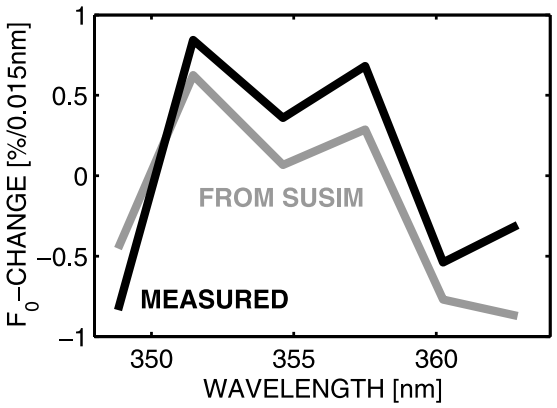

Figure 4. Percentage change of irradiance at the top of the atmosphere for a wavelength shift of +0.015 nm from Solar Ultraviolet Spectral Irradiance Monitor (SUSIM) and Brewer measurements.

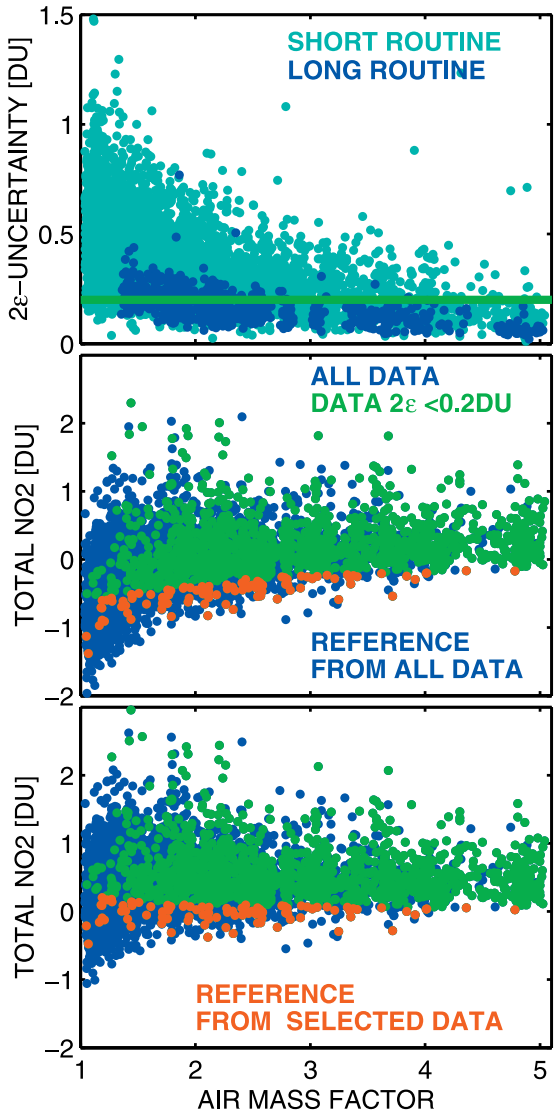

Figure 5. (top) Expanded standard error of NO_2 measurements for short and long routines. Green line indicates 0.2 DU level. (middle and bottom) Total derived NO_2 for all data (blue dots), data with standard error <0.2 DU (green dots) and reference data (red dots). Reference spectrum is taken using all data (Figure 5, middle) or reference data (Figure 5, bottom).

can estimate the offset of the grating for all measurements. When we relate the grating offset (equal to the totally correlated wavelength offset for all slits) to the measured residuals, we can determine the Brewer's proper sensitivity to F_0 (black line of Figure 4). While it is similar to the SUSIM-derived sensitivity, use of the Brewer-derived sensitivity reduces the residuals in the NO_2 retrieval.

2.3.4. Step 4

[20] We added one additional wavelength shift parameter to fit the ξ in equation (5) and fit it together with the aerosol parameters (we now have six data points and three fitting parameters). The result is much less scatter in the residuals (black dots in Figure 2), and the singular-value decomposition of the residuals approaches τ'_{NO2} (black dashed line compared to the gray line, Figure 3). This is a strong indication that the remaining influence on the residuals is mostly caused by NO_2.

2.3.5. Step 5

[21] We corrected $\ln F'_0$ by the mean of the residuals from step 4 (i.e., the mean value of the black dots in Figure 2):

$$\ln F_0^* = \ln F'_0 - \mathrm{mean}(\xi - \xi_{FIT}). \quad (7)$$

The correction from F'_0 to F_0^* should compensate for the systematic error $\Delta\ln F'_0$ but still includes the "average differential NO_2 absorption spectrum" of the database:

$$\mathrm{mean}(\xi - \xi_{FIT}) = \Delta \ln F'_0 + \tau'_{NO2}\mathrm{mean}(m_{NO2}\Omega_{NO2}). \quad (8)$$

2.3.6. Step 6

[22] Aside from the aerosol terms and the wavelength shift, we fitted the NO_2 amount Ω_{NO2} to each set ξ using the corrected F_0^* (equal to six data points, four fitting parameters). Figure 5 (middle) shows the retrieved NO_2 amounts as a function of AMF. The Ω_{NO2} are distributed around an average of zero, which is expected, since the absorption from the average NO_2 amount in the database is still contained in F_0^*.

[23] Figure 5 (top) shows the expanded standard error 2ε of the measurements, obtained from the standard deviation σ over the five sets ($2\varepsilon = 2\sigma/\sqrt{5}$). The light blue dots represent the results of the short measurement routine, where the integration time at each wavelength was 4 times less, and therefore the noise is about double the amount shown in the Figure 1 (bottom). The dark blue dots correspond to the long routine used since September 2004. The increased noise at low AMF is the main reason for the larger uncertainty of the data at low AMF compared to high AMF.

2.3.7. Step 7

[24] We select 1496 data points with less than 0.2 DU standard error from the 5310 point cloud-screened data set (green dots in Figure 5 (middle and bottom)) from the data below $2\varepsilon = 0.2$ DU (green line in Figure 5 (top)).

2.3.8. Step 8

[25] We select 100 data points with the lowest NO_2 amount. From equation (6) we can deduce that a systematic error in F_0 causes an error in the retrieved Ω_{NO2} proportional to $1/m_{NO2}$:

$$\Omega_{NO2}(\Delta \ln F'_0 = 0) = \Omega_{NO2}(\Delta \ln F'_0) + c/m_{NO2}, \quad (9)$$

where $\Omega_{NO2}(\Delta\ln F'_0 = 0)$ is the "true" vertical NO_2 column, $\Omega_{NO2}(\Delta\ln F'_0)$ is the retrieved, "false" column (data in Figure 5 (middle)), and c is a constant. In order to pick the data with the lowest true vertical column $\Omega_{NO2}(\Delta\ln F'_0 = 0)$ we have to select the data with the lowest false slant column $\Omega_{NO2}(\Delta\ln F'_0)m_{NO2}$. The selected data ("reference data") are shown as red dots in Figure 5. We assume that even in polluted sites, Ω_{NO2} is sometimes close to zero plus the small stratospheric residual. Therefore, for the reference group we assume that the last term in (8) is zero.

2.3.9. Step 9

[26] For the final F_0 we correct $\ln F'_0$ by the mean of the residuals of the reference group only. Since the mean is built from 100 data points, the noise in the mean is reduced to

Table 1. Uncertainty Budget, 2σ Standard Deviation

Source	Uncertainty
Noise (instrument and atmosphere)	
Short routine	±(0.1 to 1.0) DU ($\propto$1/m)
Long routine	±(0.1 to 0.5) DU ($\propto$1/m)
Bootstrap selection	<±0.2 DU ($\propto$1/m)
Nonlinear wavelength dependence	
Instrumental	<±0.1 DU ($\propto$1/m)
Atmospheric	±0.1 DU
Stratospheric background	−0.10 ± 0.05 DU
Other atmospheric gases	
±20 DU O_3	±0.03 DU
±1 DU HCHO	±0.05 DU
±0.002 DU BrO	±0.04 DU
Temperature profile	±0.03 DU
Surface pressure	±0.01 DU
Total uncertainty	
Short routine	−0.1 ± (0.2 to 1.0) DU
Long routine	−0.1 ± (0.2 to 0.6) DU

less than 0.01%. The final Ω_{NO2} result is shown in Figure 5 (bottom). The reference points (red dots) are close to zero. The Ω_{NO2} are mostly between 0 and 2 DU. We called this statistical approach of calibrating our instrument the bootstrap method, since the Ω_{NO2} ''pull themselves'' out of the negative values.

2.4. Uncertainty Estimation

[27] Table 1 shows the uncertainty estimation for the NO_2 retrieval. The main sources of the total uncertainty of the direct Sun retrieval (noise and bootstrap selection) decrease with increasing AMF. The largest contribution comes from the instrumental and atmospheric noise (see Figure 5, top). The uncertainty of the bootstrap selection is determined by testing the changes of Ω_{NO2} with respect to the exact selection used to determine F_0. We noticed that changing the number of reference points or limiting the range of AMF (e.g., $m_{AER} > 3$) never changed Ω_{NO2} more than 0.2 DU.

[28] As mentioned in section 2.3.3, the spectral fitting in the NO_2 retrieval includes a constant and linear term. This eliminates atmospheric and instrumental effects as long as they are linear with wavelength. However, nonlinear components will induce an error in the retrieved NO_2. Twice a day we make measurements with the Brewer's internal quartz halogen lamp in the NO_2 wavelength range for each attenuation filter. By applying the NO_2 retrieval to the lamp signals we can track a possible drift in the instrument's sensitivity or in the attenuation filters. On the basis of these tests we determined a maximum quadratic instrument sensitivity change of $\pm 1.5 \times 10^{-5}$ nm^{-2} over the whole 2 year measurement period, which causes an uncertainty in the retrieved NO_2 of ±0.10 and ±0.02 DU for AMF = 1 and 5, respectively. Since it is likely that part of this amount is due to a nonlinear change in the lamp output itself, we consider ±0.1 DU as an upper limit for the nonlinear instrumental effects at AMF = 1. We also tested the influence of the dead time correction on the NO_2 retrieval. Its influence resulted in negligible error, since the count rates are similar for all slits in this wavelength range.

[29] Both the fraction of diffuse irradiance entering the field of view (r_{SCATT}) and the aerosol extinction (τ_{AER}) may not have a perfectly linear behavior with wavelength. The influence of r_{SCATT} was estimated by taking measurements with varying fields of view. We found that the quadratic term of expression $\ln(1 - r_{SCATT})$ from equation (5) rarely exceeds $\pm 1 \times 10^{-6}$ nm^{-2} and therefore changes the retrieved NO_2 by less than ±0.01 DU. In order to estimate the influence of a nonlinear τ_{AER} we assumed a wavelength dependence according to Ångstrom's law. Varying the Ångstrom parameter α from 0 to 3 results in an NO_2 retrieval uncertainty of ±0.14 DU × τ_{AER}. On the basis of $\tau_{AER} = 0.73$, which is the 90th percentile of the aerosol extinction of the cloud-screened database, we obtain a (conservative) estimation for the NO_2 retrieval uncertainty due to nonlinear atmospheric effects (r_{SCATT} and τ_{AER}) of ±0.10 DU.

[30] The stratospheric background varies between 0.05 and 0.25 DU [*Noxon*, 1979; *Van Roozendael et al.*, 1997; *Liley et al.*, 2000]. The average stratospheric column ''included'' in the reference data (red dots in Figure 5) causes a small systematic underestimation of Ω_{NO2}. Since the reference data are a set of minimum total columns, we estimate the uncertainty from the stratospheric background to −0.10 ± 0.05 DU.

[31] The influence of other atmospheric gases, variations in the temperature profile, and surface pressure on the uncertainty are small. The uncertainty of the AMF is negligible and is not listed in Table 1.

[32] In contrast to those methods based on scattered light measurements, the total uncertainty is an absolute quantity, and therefore the relative uncertainty decreases with the total column amount. This means that the direct Sun method is more useful in polluted areas than in pristine regions. That is, while the scattered light technique has higher sensitivity for detection of NO_2, the accuracy of the direct Sun method to determine the vertical column content is better when $\Omega_{NO2} > \sim 0.5$ DU.

[33] The retrieved NO_2 amounts will change if different sets of cross sections are used for the involved absorbing gases. For example, replacing the NO_2 cross sections from *Vandaele et al.* [1998] by those from *Burrows et al.* [1998], *Voigt et al.* [2002], or *Bogumil et al.* [2003] increases the retrieved NO_2 columns by +8%, +18%, or +1%, respectively. Since we focus on the uncertainty of our measurement technique as compared to other methods, we did not include these values in the uncertainty estimation in Table 1.

2.5. Scan Data

[34] In addition to the slit mask measurements, we also took spectra in the scan mode once per day around noon. Since November 2000, we have made direct Sun scans from 289 to 363 nm at 0.5 nm step, and since September 2004, we have scanned from 347 to 363 nm at 0.1 nm step. While we applied the same analysis and calibration procedure to the scan mode data, we noticed that the NO_2 retrieval from the scan mode is much more sensitive to atmospheric variations, since the data are not taken nearly simultaneously as in the slit mask mode. This problem is worse for the 0.1 nm step scans, where there are more than 5 min between the first and the last measured wavelengths, but it is also significant for the 0.5 nm step scans, where it is just over 1 min between 347 and 363 nm. Because of this, the scan mode is useful only for a limited number of clear-sky days with excellent conditions. An example of scan mode NO_2 retrievals is given in Figure 6 for both

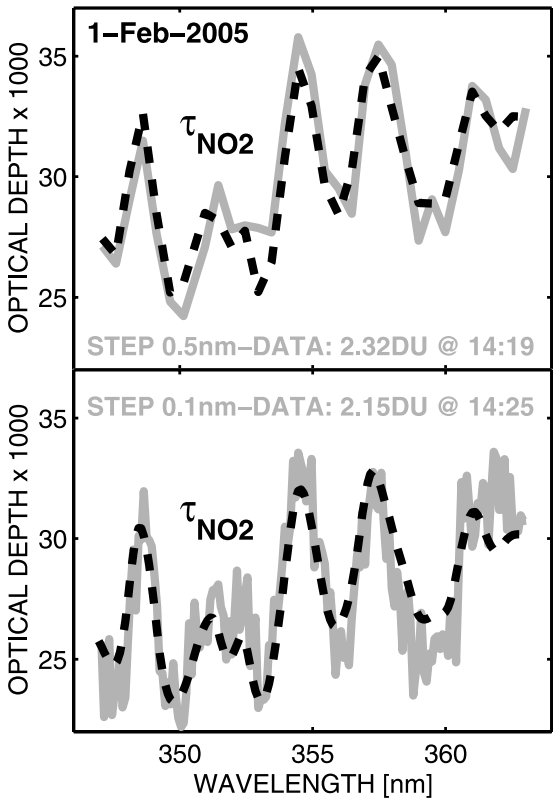

Figure 6. Retrieved NO_2 optical depths on 1 February 2005 (top) for 0.5 nm step scan and (bottom) for 0.1 nm step scan. Dashed lines are fitted NO_2 optical depths.

0.5 and 0.1 nm step scans for 1 February 2005 at 1419 and 1425 LT, respectively.

3. Results

3.1. Data Samples and Comparison With SCIAMACHY Data

[35] We are able to retrieve NO_2 column content frequently throughout the day (Figure 7). The Brewer slit mask data and expanded standard errors are represented as black symbols. The errors are significantly reduced when changing from the short routine (Figure 7, top) to the long routine (Figure 7, bottom). All samples shown are clear-sky days with excellent atmospheric conditions, and therefore the NO_2 retrievals from scan mode (gray squares) agree well with the slit mask data, validating the slit mask procedure.

[36] We have compared our NO_2 column data to those derived from measurements of the SCIAMACHY satellite instrument. SCIAMACHY was launched on European Space Agency's Envisat satellite on 28 February 2002 [*Burrows et al.*, 1995]. It is an eight-channel grating spectrometer observing the atmosphere in nadir, limb, and occultation geometry covering wavelengths from the UV to the near infrared. Column amounts and stratospheric profiles of many different trace gases can be retrieved from the measurements. Here NO_2 column amounts are derived from the nadir measurements by DOAS in the 425–450 nm fitting window (Figure 8). The total column is determined as the sum of an estimate of the stratospheric vertical column and the tropospheric column. The stratospheric contribution is derived at the same latitude over an unpolluted region using a stratospheric AMF, while the tropospheric column over the area of interest is computed using the reference sector method as described by *Richter et al.* [2004]. The tropospheric AMF is calculated on the basis of vertical NO_2 profiles simulated by the MOZART-2 chemistry transport model for 1997 [*Horowitz et al.*, 2003], using the surface reflectance for the radiative transfer calculations from the climatology of *Koelemeijer et al.* [2003]. Cloud-free scenes are selected by an intensity threshold corresponding to ~20% cloud cover. SCIAMACHY's pixel size in nadir view is about 60×30 km^2, and its overpass time is between 1000 and 1100 LT at the latitude of Washington, D. C.

[37] The gray triangles and diamonds in Figure 7 represent the SCIAMACHY measurements closest to GSFC (the distance between the ground location and SCIAMACHY pixel center is given in the legends). The NO_2 column amount shows strong variation in time (see Brewer data) and space (see SCIAMACHY data).

[38] Figure 9 compares daily means $\pm 1\sigma$ from Brewer and SCIAMACHY. The data are sorted from lowest to highest Brewer daily mean total NO_2 column. Both data sets were cloud screened, and the daily mean of the SCIAMACHY data uses all measurements within 50 km distance of the ground location. We also required at least two SCIAMACHY measurements within the 50 km, which left 56 days out of the 2 years of data for the comparison. The scatter of the ground measurements (average standard deviation of 0.3 DU) is about 3 times larger than of the satellite measurements (0.1 DU). The average total NO_2 of the Brewer measurements is 0.67 DU. For the SCIAMACHY data it depends on the selected radius around the ground location (0.41, 0.50, 0.57, and 0.62 DU for data within 200, 100, 75, and 50 km, respectively). We found that the average NO_2 amount from satellite data converges to the ground value.

[39] The correlation coefficient of the data in Figure 9 is 0.32, increasing to 0.48 if the point on the top left of the figure, marked by a square, is eliminated. Other comparisons between NO_2 data measured from ground or aircraft and space show better correlation than those presented here. *Petritoli et al.* [2004] and *Ordóñez et al.* [2006] report excellent correlation between surface NO_2 concentrations and satellite-retrieved column data. *Heue et al.* [2005] obtain excellent agreement between tropospheric NO_2 vertical columns measured from space and from aircraft-based MAXDOAS, and both *Heland et al.* [2002] and *Martin et al.* [2004] find good agreement between satellite columns and airborne in situ profiles. In section 3.2 we analyze the spatial and temporal variability of the measured NO_2, which is an important factor to understand the results of the satellite-to-ground comparison.

3.2. Spatial and Temporal Variability of NO_2

[40] The spatial variability of NO_2 can be derived from the satellite data. Figure 10 shows averaged tropospheric NO_2 columns derived from SCIAMACHY measurements for 2004. Since the main sources of anthropogenic NO_2 are traffic and industry [*Lee et al.*, 1997], the NO_2 amounts around the cities of Washington, D. C., Baltimore,

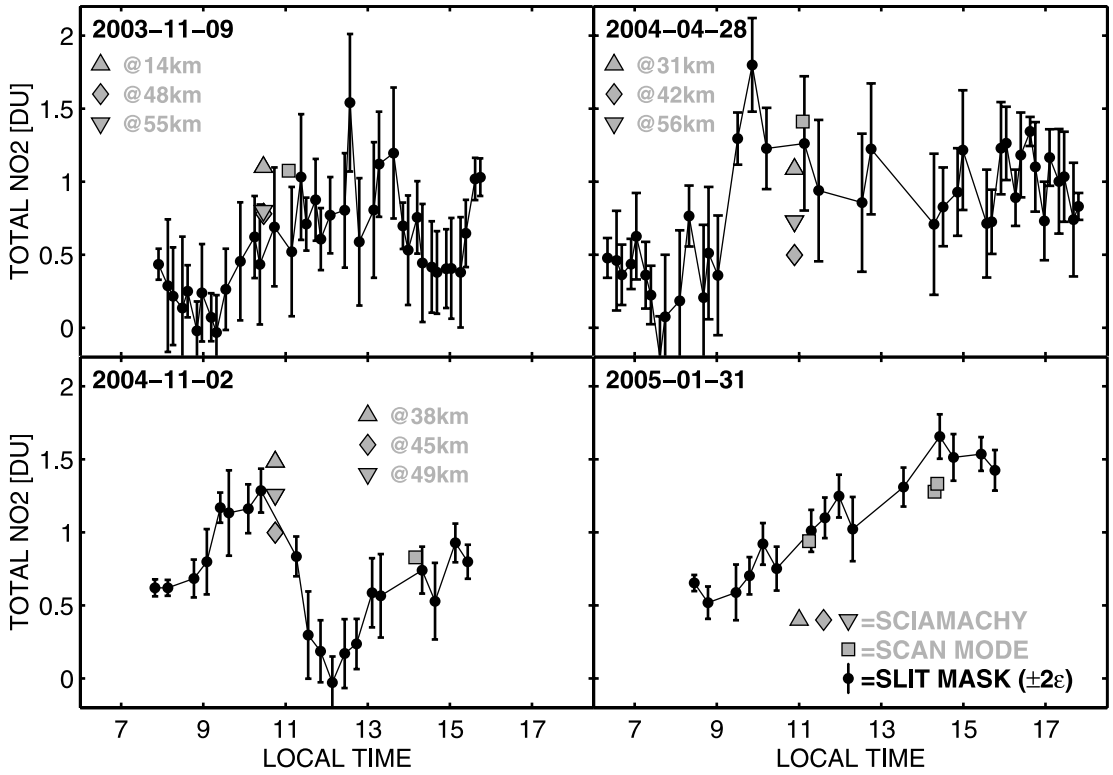

Figure 7. Total column NO_2 measurements from slit mask mode and expanded standard errors 2ε on different days (black dots and vertical bars) as a function of local standard time; gray squares show retrievals from scan mode; gray triangles and diamonds show Scanning Imaging Absorption Spectrometer for Atmospheric Chartography (SCIAMACHY) measurements (legend gives the distance between ground location and SCIAMACHY pixel center). (top) Short routine; (bottom) long routine.

Philadelphia, and New York are much higher (>0.7 DU) than in the rural environment outside the cities. From an analysis of SCIAMACHY measurements for successive pixels of the same orbit we determined the "instantaneous" spatial variability of the NO_2 column in the region. In the urban environments of Figure 10 the NO_2 column varies on an average between 0.05 and 0.1 DU/10 km, with extreme values of 0.4 DU/10 km. In rural areas the variability is mostly below 0.02 DU/10 km. On the basis of Figure 10 we have decided to use a 50 km radius for Figure 9 as the best compromise, being small enough to approach the local conditions and large enough to obtain sufficient data points.

[41] The temporal variability of NO_2 can be derived from the ground data. Figure 11 shows the dependence of total NO_2 on the time of the day. The NO_2 concentration increases until noon for all seasons. In the afternoon the

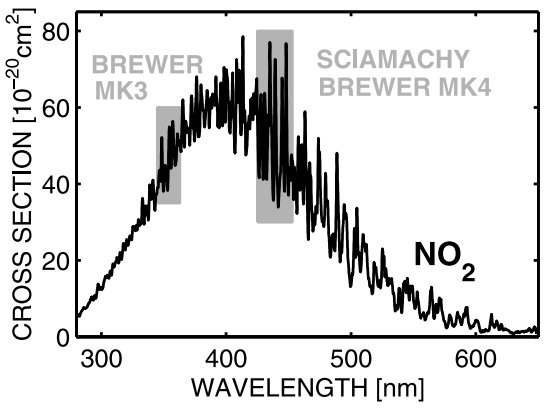

Figure 8. NO_2 absorption cross section for 294 K [*Vandaele et al.*, 1998] convoluted with a triangular slit function of 0.5 nm resolution. The gray areas represent the wavelength range used for NO_2 retrieval of (left) Brewer MK3 and (right) SCIAMACHY or Brewer MK4.

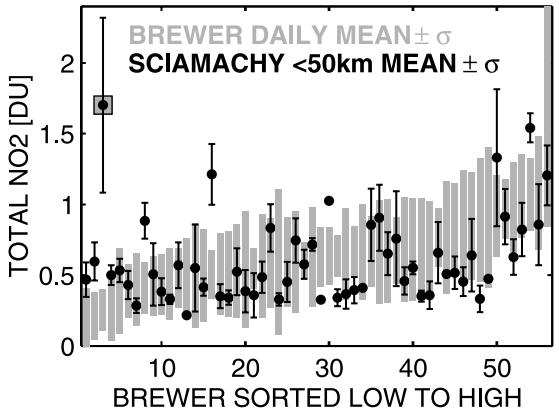

Figure 9. Brewer daily mean ± σ (gray bars) and SCIAMACHY mean ± σ within 50 km (black dots) for all cloud-screened days with at least two Brewer and SCIAMACHY measurements. The 56 data are sorted from lowest to highest Brewer daily mean.

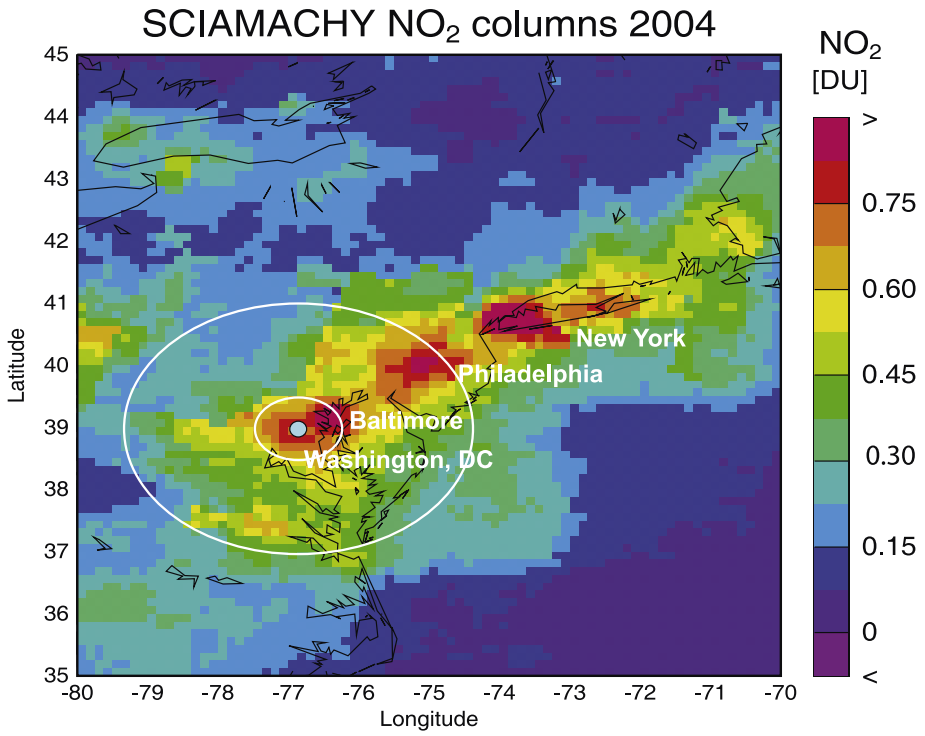

Figure 10. Averaged tropospheric NO_2 columns derived from SCIAMACHY measurements for 2004. The white ellipses show the 200 and 50 km regions around the ground location. The NO_2 hot spots coincide approximately with the locations of the labeled cities.

NO_2 amount decreases faster in the summer than in spring and fall and shows no reduction in winter. On an average the temporal variability of NO_2 is 0.1 DU h^{-1}. However, the daily courses can vary significantly from the averages shown in Figure 11 (see Figure 7). For example, on 2 November 2004, NO_2 was totally cleared out between 1000 and 1200 LT because of winds from southeast bringing unpolluted air from the ocean (Figure 7, bottom left). In this extreme situation the NO_2 amount changed at a rate of 0.7 DU h^{-1}. It is reasonable to suggest that the large temporal variability also implies significant spatial variability on scales smaller than a SCIAMACHY pixel.

[42] The diurnal patterns in Figure 11 may also be influenced by the ground measurement's viewing geometry. The direct beam crosses the atmosphere through the less populated east in the morning and the more populated west in the afternoon. However, except for very high SZA the section of the direct beam through the boundary layer, where we assume most of the NO_2 is located, is always within a few kilometers around the ground station located in a rather homogeneous suburban area. Therefore we think that the viewing geometry is not the dominant reason for the diurnal pattern.

[43] The seasonal course of NO_2 can be seen in Figure 12. It is calculated from running monthly mean data of both

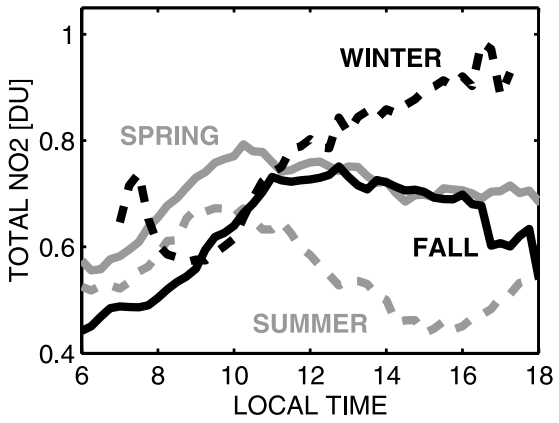

Figure 11. Running hourly mean of total NO_2 measurements for meteorological seasons.

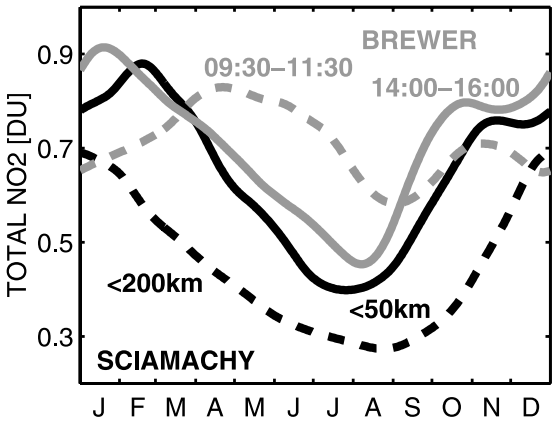

Figure 12. Smoothed seasonal cycle of total NO_2 column measured by Brewer between 0930–1130 LT (dashed gray line) and 1400–1600 LT (solid gray line) and by SCIAMACHY (~1030 LT) within 200 km (dashed black line) and 50 km (solid black line).

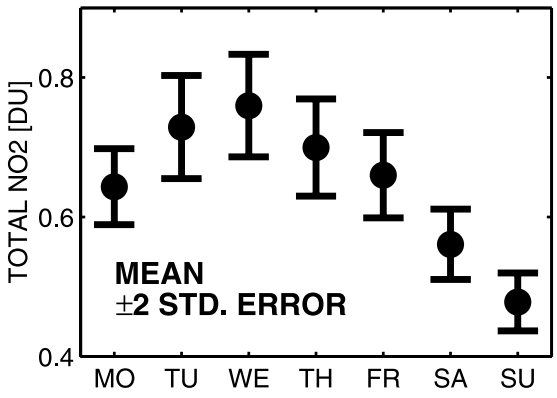

Figure 13. Total NO_2 from Brewer measurements as a function of the day of week (mean and expanded standard error).

ground (gray lines) and satellite instruments (black lines) over the 2 years of measurements and then smoothed. The satellite data show a strong seasonal cycle with minimum NO_2 amount in summer. There is a 0.2 DU difference between the 50 and 200 km regions all through the year (dashed black compared to solid black line in Figure 12, see also Figure 10). While the ground data show a significantly different seasonal cycle in the morning around SCIAMACHY's ~1030 LT overpass time (dashed gray line 0930–1130 LT), the ground-based seasonal behavior in the afternoon (solid gray line 1400–1600 LT) is close to that of the satellite (solid black line).

[44] SCIAMACHY's seasonal cycle is influenced by the vertical NO_2 profile used for the AMF calculation. On the basis of the MOZART-2 profiles the tropospheric AMF in summer is larger than in winter, reducing summer values. One possible explanation for the inconsistency of the measurements from the two instruments could be that the model profile (which is computed on a $1.8° \times 1.8°$ grid) is not typical for the measurement location or that there is a seasonality in the emissions which is not accounted for in the model. In addition, it is likely that the ground data are more representative for the region in the afternoon but are more affected by local emissions in the morning.

[45] Figure 13 shows the dependence of total NO_2 on the day of the week. Mean and expanded standard errors are calculated from daily mean values (~60 entries for each day of the week). We preferred this technique instead of averaging all single measurements (~1500 entries for each day of the week), although it increases the estimated error. The reason is that averaging all single measurements would give more weight to the summer, when the days are longer and therefore more data are taken. Averaging the daily means, we had about the same number of points in each season. The data in Figure 11 show a significant reduction of NO_2 on Saturdays and Sundays, which is attributed to reduced traffic on weekends. Figure 13 agrees closely with the analysis made by *Beirle et al.* [2003] for selected cities in the United States.

3.3. Influence of NO_2 on Aerosol Absorption Retrieval

[46] Under polluted conditions, NO_2 columns can be large, and NO_2 absorption cannot be neglected for aerosol characterization measurements. UV aerosol single-scattering albedo (SSA) has been derived from a filter instrument (UV multifilter rotating shadowband radiometer (UV-MFRSR) collocated with the Brewer) as described by *Krotkov et al.* [2005]. On 10 November 2003 the UV-MFRSR instrument measured an apparent aerosol optical depth at 368 nm of ~0.07 between 0800 and 1000 LT, increasing to ~0.15 around noon (Figure 14, top, dashed black line). Retrieving the SSA without including NO_2 absorption information resulted in unusually low SSA values between 0.65 and 0.8, which would imply an unusually high aerosol absorption coefficient (Figure 14, bottom, dashed black line). After adding the Brewer NO_2 measurements to the retrieval a large part of the apparent aerosol absorption was caused by NO_2, and the corrected SSA gave much more reasonable values between 0.8 and 0.9 (Figure 14, bottom, solid black line), consistent with the morning SSA values. This illustrates the need for simultaneous measurements of NO_2 and aerosol optical properties.

4. Summary and Conclusion

[47] In section 2 we presented a new way to derive total column atmospheric NO_2 amounts using a Brewer spectrometer in direct Sun mode. We introduced and described a statistical method to calibrate the instrument (bootstrap method). This method is based on an analysis of data obtained over an extended period (>1 year) and assumes

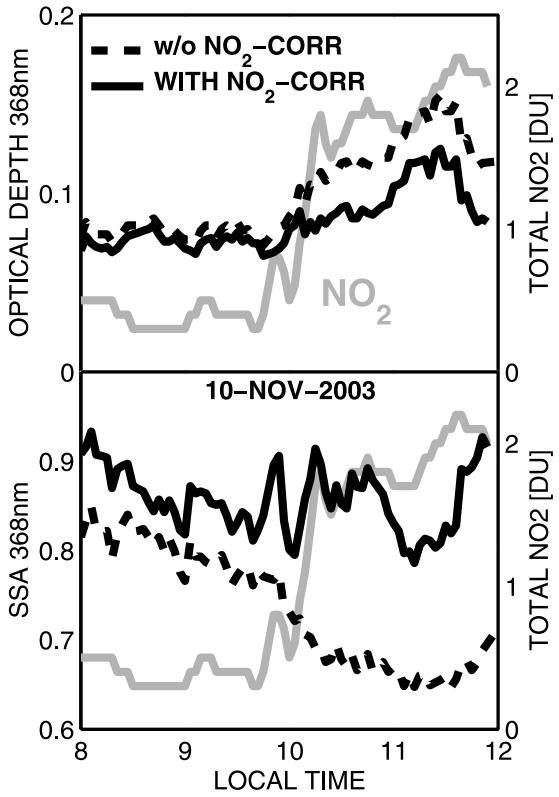

Figure 14. Total NO_2 measurements (gray line), (top) retrieved aerosol optical depth (black lines) and (bottom) single-scattering albedo (black lines) at 368 nm from a UV multifilter rotating shadowband radiometer (UV-MFRSR) on 10 November 2003 without (dashed lines) and with (solid lines) NO_2 correction.

that the NO_2 amounts are sometimes close to zero even in frequently polluted sites when meteorological conditions happen to bring in clean air. The biggest advantage of the direct Sun NO_2 retrievals is the negligible uncertainty in the AMF. That is, while scattered light measurements have higher sensitivity for detection of slant column NO_2, the accuracy of the direct Sun method to determine the total vertical column amount (troposphere plus stratosphere) is better than scattered light measurements for vertical column amounts larger than about 0.5 DU. The following points should be considered when making NO_2 measurements with Brewer spectrometers:

[48] 1. Instead of applying the bootstrap method, one could also move the instrument to a clean site with very small tropospheric NO_2 concentration (e.g., a high-altitude mountain station). From previous limited experience the Brewer 171 instrument appears to be stable enough to do this without the calibration changing significantly because of transport. This observation probably also applies to other Brewer instruments.

[49] 2. It is important to include the O_2-O_2 absorption in the algorithm. Otherwise a false AMF dependence of the NO_2 retrievals is introduced.

[50] 3. Although the Brewer's wavelength uncertainty of 0.015 nm is rather small, it is still large enough to influence the NO_2 retrieval. Therefore a wavelength shift parameter must be fitted to the data. Since there is practically no spectrum stretching in the Brewer [*Gröbner et al.*, 1998] and the slits are totally correlated concerning wavelength shift (slits are cut into a rigid plate), no stretching parameter has to be used.

[51] 4. Since NO_2 retrievals are very sensitive to temporal variations in the atmosphere over short timescales (a few seconds), all wavelengths should be measured (nearly) simultaneously. Classical scanning techniques only work for a very limited number of clear-sky days with excellent stable conditions. Since we have demonstrated that the slit mask measurements match the scanning measurements on clear days, we suggest that the optimum procedure for Brewer NO_2 measurements is to use the slit mask mode rather than the scan mode.

[52] 5. In this paper we made an absolute calibration of the Brewer in the laboratory and used the SUSIM/Atlas 3 spectrum, corrected for the Sun-Earth distance, as a first guess for the irradiance at the top of the atmosphere (F_0'). It is also possible to use the instrument's effective count rates in the algorithm instead. The first guess F_0' may be obtained by Langley calibrations in that case.

[53] 6. The method described in this paper should also work for single-monochromator-type Brewers, since the spectral stray light in this wavelength range is of minor importance and affects all wavelengths in approximately the same way. The MK4 Brewer types using the grating's second order of scattering between 428 and 453 nm have the advantage of larger structure in the NO_2 cross section compared to the UV (see Figure 8) and therefore improved sensitivity. However, care should be taken in the inclusion of slit 4 (442.8 nm) since this wavelength is influenced by water vapor absorption.

[54] 7. Our future plans include comparisons of the Brewer NO_2 retrievals with collocated in situ aircraft and/or balloon measurements.

[55] In section 3 we analyzed 2 years of NO_2 measurements in Washington, D. C., compared them to satellite data from SCIAMACHY, and determined the spatial and temporal variability of atmospheric NO_2 in the region. We also showed that high NO_2 levels strongly influence the determination of aerosol absorption properties. The following observations have been made:

[56] 1. Both ground and satellite data measure an average NO_2 column of about 0.7 DU at GSFC.

[57] 2. On an average, the NO_2 concentration at GSFC increases from sunrise to noon. In the afternoon it decreases quicker in summer than in other seasons.

[58] 3. While the ground data show a significantly different seasonal cycle in the morning, the ground-based seasonal behavior in the afternoon is close to that of the satellite, with higher NO_2 columns in winter than in summer. Possibly the ground data are more representative of the larger region in the afternoon and are more affected by local emissions in the morning.

[59] 4. The spatial and temporal variabilities of the measured NO_2 column over GSFC are on an average 0.1 DU/10 km and 0.1 DU h^{-1} with extreme values of 0.4 DU/10 km and 0.7 DU h^{-1}, respectively.

[60] 5. The day-to-day variability of the temporal total NO_2 behavior at GSFC is large. Depending on the wind direction, more polluted air from the city and nearby highways or cleaner air from the less populated ocean direction can be transported to the site.

[61] 6. The correlation of daily data from ground and satellite is poor. We attribute this to the high temporal and spatial variability of NO_2 in this region in combination with the different viewing geometries of ground and satellite instruments. While NO_2 columns retrieved from SCIAMACHY are a true average over the satellite's field of view, the Brewer measurements are of very local nature.

[62] 7. The NO_2 amounts at GSFC are reduced on Saturdays and even more on Sundays because of reduced traffic on weekends.

[63] 8. We showed that NO_2 should be considered when retrieving aerosol absorption, especially for situations with low aerosol optical depth. NO_2 absorption will affect SSA retrievals in the UV and visible from Sun photometers such as those used by Aerosol Robotic Network (AERONET) [*Dubovik et al.*, 2000]. Neglect of NO_2 will lead to overestimation of aerosol absorption, mainly in the range from ~360 to ~450 nm (see Figure 8).

[64] **Acknowledgments.** We would like to thank the people involved in the operation and calibration of the Brewer spectrometer and the coworkers in the Atmospheric Chemistry and Dynamics Branch at GSFC for their useful comments. SCIAMACHY lv0 and lv1 spectra were provided by ESA through DFD/DLR.

References

Beirle, S., U. Platt, M. Wenig, and T. Wagner (2003), Weekly cycle of NO_2 by GOME measurements: A signature of anthropogenic sources, *Atmos. Chem. Phys.*, *3*, 2225–2232.

Bodhaine, B. A., N. B. Wood, E. G. Dutton, and J. R. Slusser (1999), On Rayleigh optical depth calculations, *J. Atmos. Oceanic Technol.*, *16*, 1854–1861.

Boersma, K. F., H. J. Eskes, and E. J. Brinksma (2004), Error analysis for tropospheric NO_2 retrieval from space, *J. Geophys. Res.*, *109*, D04311, doi:10.1029/2003JD003962.

Bogumil, K., et al. (2003), Measurements of molecular absorption spectra with the SCIAMACHY pre-flight model: Instrument characterization and

reference data for atmospheric remote-sensing in the 230–2380 nm region, *J. Photochem. Photobiol. A*, *157*, 167–184.

Brewer, A. W., C. T. McElroy, and J. B. Kerr (1973), Nitrogen dioxide concentrations in the atmosphere, *Nature*, *246*(5429), 129–133.

Burrows, J. P., E. Hölzle, A. P. H. Goede, H. Visser, and W. Fricke (1995), SCIAMACHY-Scanning Imaging Absorption Spectrometer for Atmospheric Chartography, *Acta Astronaut.*, *35*, 445–451.

Burrows, J. P., A. Dehn, B. Deters, S. Himmelman, A. Richter, S. Voigt, and J. Orphal (1998), Atmospheric remote sensing reference data from GOME: part 1. Temperature dependent absorption cross-sections of NO_2 in the 231–794 nm range, *J. Quant. Spectrosc. Radiat. Transfer*, *60*, 1025–1031.

Burrows, J. P., A. Richter, A. Dehn, B. Deters, S. Himmelmann, S. Voigt, and J. Orphal (1999), Atmospheric remote-sensing reference data from GOME—2. Temperature-dependent absorption cross sections of O_3 in the 231–794 nm range, *J. Quant. Spectrosc. Radiat. Transfer*, *61*, 509–517.

Dubovik, O., A. Smirnov, B. N. Holben, M. D. King, Y. L. Kaufmann, T. F. Eck, and I. Slutsker (2000), Accuracy assessments of aerosol optical properties retrieved from Aeronet Robotic Network (AERONET) Sun and sky radiance measurements, *J. Geophys. Res.*, *105*(D8), 9791–9806.

Environmental Protection Agency (1998), National air quality and emissions trends report 1997, Research Triangle Park, N. C.

Floyd, L. E., J. W. Cook, L. C. Herring, and P. C. Crane (2003), SUSIM'S 11-year observational record of the solar UV irradiance, *Adv. Space Res.*, *31*, 2111–2120.

Francesconi, M., G. R. Casale, A. M. Siani, and S. Casadio (2004), Ground-based NO_2 measurements at the Italian Brewer stations: A pilot study with Global Ozone Monitoring Experiment (GOME), *Nuovo Cimento Soc. Ital. Fis. C*, *27*(4), 383–392, doi:10.1393/ncc/i2004-10036-8.

Greenblatt, G. D., J. J. Orlando, J. B. Burkholder, and A. R. Ravishankara (1990), Absorption measurements of oxygen between 330 and 1140 nm, *J. Geophys. Res.*, *95*(D11), 18,577–18,582.

Gröbner, J., D. I. Wardle, C. T. McElroy, and J. B. Kerr (1998), Investigation of the wavelength accuracy of Brewer spectrophotometers, *Appl. Opt.*, *37*(36), 8352–8360.

Heckel, A., A. Richter, T. Tarsu, F. Wittrock, C. Hak, I. Pundt, W. Junkermann, and J. P. Burrows (2005), MAX-DOAS measurements of formaldehyde in the Po-Valley, *Atmos. Chem. Phys.*, *5*, 909–918.

Heland, J., H. Schlager, A. Richter, and J. P. Burrows (2002), First comparison of tropospheric NO_2 column densities retrieved from GOME measurements and in situ aircraft profile measurements, *Geophys. Res. Lett.*, *29*(20), 1983, doi:10.1029/2002GL015528.

Heue, K.-P., A. Richter, T. Wagner, M. Bruns, J. P. Burrows, C. von Friedeburg, W. D. Lee, U. Platt, I. Pundt, and P. Wang (2005), Validation of SCIAMACHY tropospheric NO_2-columns with AMAXDOAS measurements, *Atmos. Chem. Phys.*, *5*, 1039–1051.

Horowitz, L. W., et al. (2003), A global simulation of tropospheric ozone and related tracers: Description and evaluation of MOZART, version 2, *J. Geophys. Res.*, *108*(D24), 4784, doi:10.1029/2002JD002853.

Kazadzis, S., A. Bais, N. Kouremeti, E. Gerasopoulos, K. Garane, M. Blumthaler, B. Schallhart, and A. Cede (2005), Direct spectral measurements with a Brewer spectroradiometer: Absolute calibration and aerosol optical depth retrieval, *Appl. Opt.*, *44*(9), 1681–1690.

Kerr, J. B., C. T. McElroy, D. I. Wardle, R. A. Olafson, and W. F. J. Evans (1985), The automated Brewer spectrophotometer, in *Atmospheric Ozone: Proceedings of the Quadrennial Ozone Symposium*, edited by C. S. Zerefos and A. Ghazi, pp. 396–401, Springer, New York.

Koelemeijer, R. B. A., J. F. de Haan, and P. Stammes (2003), A database of spectral surface reflectivity in the range 335–772 nm derived from 5.5 years of GOME observations, *J. Geophys. Res.*, *108*(D2), 4070, doi:10.1029/2002JD002429.

Krotkov, N., P. K. Bhartia, J. Herman, J. Slusser, G. Scott, G. Labow, A. P. Vasilkov, T. F. Eck, O. Dubovik, and B. N. Holben (2005), Aerosol ultraviolet absorption experiment (2002 to 2004), part 2: Absorption optical thickness, refractive index, and single scattering albedo, *Opt. Eng.*, *44*(4), 041005, 1–17.

Lee, D. S., I. Köhler, E. Grobler, F. Rohrer, R. Sausen, L. Gallardo-Klenner, J. G. J. Olivier, F. J. Dentener, and A. F. Bouwman (1997), Estimations of global NO_x emissions and their uncertainties, *Atmos. Environ.*, *31*, 1735–1749.

Leser, H., G. Hönninger, and U. Platt (2003), MAX-DOAS measurements of BrO and NO_2 in the marine boundary layer, *Geophys. Res. Lett.*, *30*(10), 1537, doi:10.1029/2002GL015811.

Leue, C., M. Wenig, T. Wagner, O. Klimm, U. Platt, and B. Jähne (2001), Quantitative analysis of NO_x emissions from Global Ozone Monitoring Experiment satellite image sequences, *J. Geophys. Res.*, *106*(D6), 5493–5505.

Liley, J. B., P. V. Johnston, R. L. McKenzie, A. J. Thomas, and I. S. Boyd (2000), Stratospheric NO_2 variations from a long time series at Lauder, New Zealand, *J. Geophys. Res.*, *105*(D9), 11,633–11,640.

Martin, R. V., et al. (2004), Evaluation of GOME satellite measurements of tropospheric NO_2 and HCHO using regional data from aircraft campaigns in the southeastern United States, *J. Geophys. Res.*, *109*, D24307, doi:10.1029/2004JD004869.

Meller, R., and G. K. Moortgat (2000), Temperature dependence of the absorption cross sections of formaldehyde between 223 and 323 K in the wavelength range 225–375 nm, *J. Geophys. Res.*, *105*(D6), 7089–7101.

Noxon, J. F. (1979), Stratospheric NO_2: 2. Global behavior, *J. Geophys. Res.*, *84*(C8), 5067–5076.

Ordóñez, C. A., et al. (2006), Comparison between 7 years of satellite-borne and ground-based tropospheric NO_2 measurements around Milan, Italy, *J. Geophys. Res.*, doi:10.1029/2005JD006305, in press.

Petritoli, A., P. Bonasoni, G. Giovanelli, F. Ravegnani, I. Kostadinov, D. Bortoli, A. Weiss, D. Schaub, A. Richter, and F. Fortezza (2004), First comparison between ground-based and satellite-borne measurements of tropospheric nitrogen dioxide in the Po basin, *J. Geophys. Res.*, *109*, D15307, doi:10.1029/2004JD004547.

Platt, U. (1994), Differential Optical Absorption Spectroscopy (DOAS), in *Air Monitoring by Spectroscopic Techniques*, *Chem. Anal.*, vol. 127, edited by M. W. Sigrist, pp. 27–84, John Wiley, Hoboken, N. J.

Richter, A., and J. P. Burrows (2002), Tropospheric NO_2 from GOME measurements, *Adv. Space Res.*, *29*, 1673–1683.

Richter, A., V. Eyring, J. P. Burrows, H. Bovensmann, A. Lauer, B. Sierk, and P. J. Crutzen (2004), Satellite measurements of NO_2 from international shipping emissions, *Geophys. Res. Lett.*, *31*, L23110, doi:10.1029/2004GL020822.

Roscoe, H. K., et al. (1999), Slant column measurements of O_3 and NO_2 during the NDSC intercomparison of zenith-sky UV-visible spectrometers in June 1996, *J. Atmos. Chem.*, *32*, 281–314.

Rublev, A. N., N. E. Chubarova, A. N. Trotsenko, and G. I. Gorchakov (2003), Determination of NO_2 column amounts from AERONET data, *Izv. Atmos. Oceanic Phys.*, *40*(1), 54–67.

Solomon, S., A. L. Schmeltekopf, and R. W. Sanders (1987), On the interpretation of zenith sky absorption measurements, *J. Geophys. Res.*, *92*(D7), 8311–8319.

Solomon, S., R. W. Portmann, R. W. Sanders, J. S. Daniel, W. Madsen, B. Bartram, and E. G. Dutton (1999), On the role of nitrogen dioxide in the absorption of solar radiation, *J. Geophys. Res.*, *104*(D10), 12,047–12,058.

Vandaele, A. C., P. C. Simon, J. M. Guilmot, M. Carleer, and R. Colin (1994), SO_2 absorption cross section measurement in the UV using a Fourier transform spectrometer, *J. Geophys. Res.*, *99*(D12), 25,599–25,606.

Vandaele, A. C., C. Hermans, P. C. Simon, M. Carleer, R. Colin, S. Fally, M. F. Mérienne, A. Jenouvrier, and B. Coquart (1998), Measurements of the NO_2 absorption cross-section from 42,000 cm^{-1} to 10,000 cm^{-1} (238–1000 nm) at 220 K and 294 K, *J. Quant. Spectrosc. Radiat. Transfer*, *59*, 171–184.

Vandaele, A. C., et al. (2005), An intercomparison campaign of ground-based UV-visible measurements of NO_2, BrO, and OClO slant columns: Methods of analysis and results for NO_2, *J. Geophys. Res.*, *110*, D08305, doi:10.1029/2004JD005423.

Van Roozendael, M., M. de Mazière, C. Hermans, P. C. Simon, J. P. Pommereau, F. Goutail, X. X. Tie, G. Brasseur, and C. Granier (1997), Ground-based observations of stratospheric NO_2 at high and midlatitudes in Europe after the Mount Pinatubo eruption, *J. Geophys. Res.*, *102*(D15), 19,171–19,176.

Velders, G. J. M., C. Granier, R. W. Portmann, K. Pfeilsticker, M. Wenig, T. Wagner, U. Platt, A. Richter, and J. P. Burrows (2001), Global tropospheric NO_2 column distributions: Comparing three-dimensional model calculations with GOME measurements, *J. Geophys. Res.*, *106*(D12), 12,643–12,660.

Voigt, S., J. Orphal, and J. P. Burrows (2002), The temperature- and pressure-dependence of the absorption cross-sections of NO_2 in the 250–800 nm region measured by Fourier-transform spectroscopy, *J. Photochem. Photobiol. A*, *149*, 1–7.

Wilmouth, D. M., T. F. Hanisco, N. M. Donahue, and J. G. Anderson (1999), Fourier transform ultraviolet spectroscopy of the $A^2_{3/2}$ $X^2_{3/2}$ transition of BrO, *J. Phys. Chem. A*, *103*, 8935–8945.

J. Burrows and A. Richter, Institute of Environmental Physics, University of Bremen, Postfach 330440, D-28344 Bremen, Germany.

A. Cede, J. Herman, and N. Krotkov, NASA GSFC, Code 613.3, 8800 Greenbelt Road, Greenbelt, MD 20771-0000, USA. (cede@gsfc.nasa.gov)